SCHOOL OF MATHEMATICAL SCIENCES

UNIVERSITY OF MELBOURNE

Nonlinear internal gravity waves and their interaction with the mean wind

by

R. GRIMSHAW

RESEARCH REPORT No. 2 1975

ISBN 0 86890 043 5

NONLINEAR INTERNAL GRAVITY WAVES AND THEIR INTERACTION WITH THE MEAN WIND

R. GRIMSHAW

Mathematics Department, University of Melbourne

Parkville, Victoria 3052, Australia

National Library of Australia card number and ISBN 0 86890 043 5

ABSTRACT

The interaction of a wave packet of internal gravity waves with the mean wind is investigated, for the case when there is a region of wind shear and hence a critical level. The principal equations are the Doppler-shifted dispersion relation, the equation for conservation of wave action and the mean momentum equation, in which the mean wind is accelerated by a "radiation stress" tensor, due to the waves. These equations are integrated numerically to study the behaviour of a wave packet approaching a critical level, where the horizontal phase speed matches the mean wind. The results demonstrate the exchange of energy from the waves to the mean wind in the vicinity of the critical level. The interaction between the waves and the mean wind is also studied in the absence of any initial wind shear.

§1. INTRODUCTION

It is well known that internal gravity waves are an important and ubiquitous feature of the atmosphere. Because the density of the atmosphere decreases continuously with height, these waves have a propensity for an exponential growth of amplitude with height. Consequently, any linearised model for internal gravity waves must eventually fail, and nonlinear aspects must be considered. Hines (1972) has drawn attention to the important role these waves play in the transfer of momentum from one part of the atmosphere to another. Momentum transfer is likely to be associated with such factors as turbulence, dissipation (due to molecular viscosity and heat conduction), ionisation and conductivity (at heights greater than 100 km.), reflection processes (associated with sharp changes in the density and wind profiles), and critical layer absorption (at a level where the mean wind speed is matched by the horizontal phase speed of the waves). In this paper we are principally concerned with critical layer absorption.

Gossard et.al. (1970) have observed gravity waves propagating towards a critical level, where their absorption is associated with a region of instability. Booker and Bretherton (1967) have shown that when an internal gravity wave propagates through a region of wind shear (the mean wind varying continuously with height), the vertical flux of horizontal momentum will be constant with height, except at critical levels where the waves are attenuated by a factor

$$\exp\{-2\pi(R_c - \tfrac{1}{4})^{\frac{1}{2}}\} , \qquad (1.1)$$

where R_c is the Richardson number at the critical level. The local

Richardson number is

$$R = N^2/U_z^2 + V_z^2 , \qquad (1.2)$$

where N^2 is the Brunt-Väisälä frequency, and (U(z),V(z),0) is the mean horizontal velocity. It was assumed that R is greater than ¼, as this is a sufficient condition for the stability of the mean flow. The importance of critical layers was also postulated by Hines and Reddy (1967), who used a multi-layered representation of the wind shear. However, these linearised theories also predict infinite wave amplitudes at the critical level, and thus nonlinear theories must be invoked. Jones and Houghton (1971) developed a numerical model to describe the coupling between internal gravity waves and the mean wind; the linearised equations were coupled to the mean wind by allowing the gradient of the wave momentum flux to produce accelerations of the mean wind. They found a shelf developing in the mean wind profile in the vicinity of the critical level. Breeding (1971) used a numerical model of the nonlinear equations, and also found a shelf near the critical level, although the Richardson number was smaller than that used by Jones and Houghton. Lindzen and Holton (1968) have invoked critical layer absorption in a discussion of the quasi-biennial oscillation; their numerical procedure amounts to making an ad hoc assumption about the coupling between the wave momentum flux and the mean wind.

Large amplitude internal gravity waves can cause changes in the mean wind even in the absence of any initial shear; these changes may then introduce a critical level causing absorption, or

"self-destruction", of the gravity wave. This process has been examined numerically by Jones and Houghton (1972) and Breeding (1972).

In the present paper these phenomenon are studied using the notion of a wave packet interacting with the mean wind. This approach assumes that the properties of the mean state of the atmosphere vary slowly on a length scale determined by the local wave structure, and is thus a large Richardson number approximation. The equations describing the behaviour of the wave packet are obtained by a multiple-scaling technique (partly described by averaging the equations of motion over a wavelength). These equations have been derived elsewhere (Grimshaw 1972, 1974) and will be stated and discussed in §2. A simplified version of the equations has been integrated numerically and the results are given in §3. The finite difference scheme used for the numerical calculations is described in Appendix A.

§2. EQUATIONS DETERMINING THE INTERACTION OF A WAVE PACKET WITH THE MEAN WIND

These equations are

$$\omega^* = \omega - \underset{\sim}{\kappa}_H \cdot \underset{\sim}{V} , \tag{2.1}$$

$$\omega^{*2} = N^2 \kappa_H^2 / \kappa^2 , \tag{2.2}$$

$$\underset{\sim}{\kappa}_T + \nabla\omega = 0, \ \text{curl}\ \underset{\sim}{\kappa} = 0, \tag{2.3}$$

$$\nabla_H \cdot \underset{\sim}{V} = 0 , \tag{2.4}$$

$$\rho_0 \frac{D\underset{\sim}{V}}{DT} + \nabla.(\mathcal{J}\underset{\sim}{c}\underset{\sim}{\kappa}_H) + \nabla_H Q = 0 , \tag{2.5}$$

$$\frac{D\mathcal{J}}{DT} + \nabla.(\mathcal{J}\underset{\sim}{c}) + \lambda\kappa^2\mathcal{J} = 0 , \tag{2.6}$$

$$\frac{D}{DT} \equiv \frac{\partial}{\partial T} + \underset{\sim}{V}.\nabla_H . \tag{2.7}$$

They are derived in Grimshaw (1974, §4) (see also Grimshaw (1972) for an alternative derivation which ignores dissipative effects). Here $\underset{\sim}{V}$ is the horizontal component of the mean wind, $\rho_0(Z)$ is the mean density (varies only with height Z), $N^2(Z)$ is the Brunt-Väisälä frequency, and $\nabla_H Q$ is the mean horizontal pressure gradient. The parameters describing the wave packet are ω, the local frequency, $\underset{\sim}{\kappa}$, the local wavenumber vector, ($\kappa = |\underset{\sim}{\kappa}|$ is its magnitude, $\underset{\sim}{\kappa}_H$ is the horizontal component of $\underset{\sim}{\kappa}$ and $\kappa_H = |\underset{\sim}{\kappa}_H|$), and ω^* (2.1) is the intrinsic (Doppler-shifted) frequency; (2.2) is the familiar dispersion relation for internal gravity waves, and $\underset{\sim}{c}$ is the group velocity

$$\underset{\sim}{c} = \nabla_{\underset{\sim}{\kappa}} \omega^* . \tag{2.8}$$

It is well known that $\underset{\sim}{c}$ is perpendicular to $\underset{\sim}{\kappa}$, so that waves whose energy is propagating vertically upwards will have phase velocities

which are vertically downwards. (2.3) describes the conservation of waves; it is most simply derived from the observation that, in terms of the phase of the waves $\Theta(\underset{\sim}{X},T)$, ω is $-\Theta_T$ and $\underset{\sim}{k}$ is $\nabla\Theta$. The amplitude of the waves is described by the wave action density

$$\mathcal{A} = \mathcal{E}/\omega^* , \qquad (2.9)$$

where $\mathcal{E}$ is the wave energy density. Dissipative effects are represented by the dissipation parameter λ, which is defined below. In the equations (2.1) to (2.7), and hereafter, a subscript H denotes horizontal component.

The fifth equation (2.5) describes the acceleration of the mean wind by the action of a "radiation stress tensor", $\mathcal{T}_{\underset{\sim}{c}\underset{\sim}{k}_H}$. It is shown in Grimshaw (1974) that

$$\mathcal{T}_{\underset{\sim}{c}\underset{\sim}{k}_H} = \langle \rho_0 \underset{\sim}{v} v_H \rangle \qquad (2.10)$$

where angle brackets denote an average over the wave, and $\underset{\sim}{v}$ is the velocity of the wavelike perturbations. Thus, in the present context, $\mathcal{T}_{\underset{\sim}{c}\underset{\sim}{k}_H}$ is just that component of the Reynolds stress which can exert a force in a horizontal direction. The sixth equation (2.6) is the equation for conservation of wave action (cf. Bretherton and Garrett (1969)). As remarked in §1, these equations are derived by a multiple-scaling technique, which assumes that the local wavelength is much smaller than the length scale associated with the mean wind. Thus, locally, the equations of motion reduce to those which describe internal gravity waves in the incompressible, inviscid limit; the interaction of the waves with the mean wind occurs on the long length

scale, and the equations (2.1) and (2.7) may, for the present purposes, be regarded as the result of removing the short length scale by averaging over a wavelength. It should be emphasised here that these equations are fully nonlinear, and there has been no restriction made on the size of the wave amplitude. The effects of rotation have not been included. (cf. Grimshaw (1975) for analysis of the equations which arise when rotation is included.)

The equations are expressed in terms of non-dimensional co-ordinates. Thus we let L_1 be a length scale characterising a wavelength, and N_1^{-1} be a time scale, where N_1 is a typical value of the Brunt-Väisälä frequency and of the wave period. Then the long length scale is chosen to be gN_1^{-2}, and

$$\varepsilon = N_1^2 L/g \tag{2.11}$$

is the small parameter which is the ratio of the short length scale to the long length scale. In terms of this scaling, the Richardson number (1.2) is $O(\varepsilon^{-2})$. Equations (2.1) to (2.7) have independent non-dimensional variables $\underset{\sim}{X}$, T which are related to the corresponding dimensional variables $\underset{\sim}{x}$, t say, by

$$\underset{\sim}{X} = \varepsilon \underset{\sim}{x}/L_1 \ , \quad T = \varepsilon N_1 t \ . \tag{2.12}$$

All velocities have been scaled by $N_1 L_1$, the density by ρ_1 and the pressure by $\rho_1 N_1^2 L_1^2$. In terms of these scalings, the dissipation parameter is

$$\lambda = \frac{E}{\varepsilon} (\nu_0 + \sigma k_0) \ , \tag{2.13}$$

where $$E = \nu_1/N_1 L_1^2 \ .$$

Here ν_1 is a typical scale for the kinematic viscosity, and so E is an inverse Reynolds number; σ is the Prandtl number, and ν_0, k_0 (functions of Z only) are the dimensionless kinematic viscosity and thermal diffusivity respectively. In terms of this scaling, the vertical compenent of the mean wind is $O(\varepsilon^2)$; also, all the equations (2.1) to (2.7) have relative errors of $O(\varepsilon)$. Although we shall be using the non-dimensional variables, it may be noted that a reversion to dimensional co-ordinates would leave the form of (2.1) to (2.7) unchanged. Also, a further arbitrary scaling of the time variable T by t_1, the space variable $\underset{\sim}{X}$ by ℓ_1, and the density by ρ_1 would leave the equations (2.1) to (2.7) unchanged provided that $\mathcal{F}$ and Q are simultaneously scaled by $\rho_1 \ell_1^2 t_1^{-1}$, and λ is scaled by $\ell_1^2 t_1^{-1}$. Thus, in the numerical work, we are free to select the length and time scales; in practice (see §3), the length scale is selected arbitrarily, and then λ is chosen so that the wave packet has time to propagate to the critical level before significant interactions with the mean wind take place.

The manner in which the mean momentum equation (2.5) describes the production of mean vorticity by the "radiation stress" tensor associated with the wave packet has been described in Grimshaw (1974). Briefly

$$\frac{D}{DT} \oint_{\mathcal{C}} \underset{\sim}{V}.d\underset{\sim}{X} = \frac{D}{DT} \oint_{\mathcal{C}} \underset{\sim}{U}.d\underset{\sim}{X} + \oint_{\mathcal{C}} \lambda\kappa^2 \underset{\sim}{U}.d\underset{\sim}{X} \ , \qquad (2.14)$$

where $$\underset{\sim}{U} = \underset{\underset{\sim}{H}}{\kappa} \mathcal{F}/\rho_0 \ , \qquad (2.15)$$

where $\mathcal{C}$ is a circuit moving with the mean wind. The first term describes the instantaneous production of mean vorticity in the vicinity of a wave packet, while the second term describes the permanent production of vorticity associated with dissipation of the wave packet. Here, however, we propose to examine a simpler situation, in which all the variables in (2.1) to (2.7) are functions only of the height Z, and the time T. This corresponds, for example, to a situation in which internal gravity waves are produced by a forcing mechanism in a horizontal plane, in which the forcing term is periodic in both horizontal co-ordinates. (If the forcing term does not extend to infinity in the horizontal plane, then the resulting wave packet will have horizontal gradients of the "radiation stress" tensor at its horizontal boundaries; however, if the wave packet is of much larger horizontal extent than vertical extent, the mean velocities generated by these horizontal gradients will be smaller than those generated by the vertical gradients, and will be confined to the vicinity of the horizontal boundaries.) The resulting equations are (2.1), (2.2) and

$$n_T + \omega_Z = 0, \tag{2.16}$$

$$\rho_0 \underset{\sim}{V}_T + (\mathcal{F}_W)_Z \underset{\sim}{\kappa}_H = 0, \tag{2.17}$$

$$\mathcal{F}_T + (\mathcal{F}_W)_Z + \lambda \kappa^2 \mathcal{F} = 0, \tag{2.18}$$

where

$$W = \frac{\partial \omega^*}{\partial n} = - \frac{n\omega^*}{\kappa^2} . \tag{2.19}$$

Here n is the vertical component of $\underset{\sim}{\kappa}$, and W is the vertical component of group velocity $\underset{\sim}{c}$; also (2.3) shows that $\underset{\sim}{\kappa}_H$ is a constant. Since ω (by virtue of (2.1) and (2.2)) is a known function of n and $\underset{\sim}{V}$ (also of Z through its dependence on N^2), these constitute three equations for n, $\underset{\sim}{V}$ and $\mathcal{F}$. It is these equations which have been integrated

numerically, and the results described in §3. They are inextricably coupled; (2.17) describes the change in $\underset{\sim}{V}$ due to changes in $\mathcal{F}$, and then (2.1) and (2.16) describe the resulting change in n due to changes in $\underset{\sim}{V}$; the change in n then acts as feed-back to change $\mathcal{F}$, as W depends on n.

Before discussing the numerical results, we shall close this section by exhibiting the solution of (2.16), (2.17) and (2.18) in the small amplitude limit. In this limit ($\mathcal{F} \to 0$), (2.17) is ignored, and $\underset{\sim}{V}$ is assumed to be prescribed for all time; then (2.16) is an equation for n alone, and once n has been found, $\mathcal{F}$ can be determined by integrating (2.18). The procedure is discussed in Grimshaw (1972, 1974). For example, let N^2 be a constant, and

$$\underset{\sim}{V} = \beta Z \underset{\sim}{i} \ , \tag{2.20}$$

where $\underset{\sim}{i}$ is a unit vector in the X-direction, and let initially at T = 0 say, ω be a constant ω_0 (i.e. the source producing the wave packet is operating at constant frequency). Then

$$\omega^* = \ell\beta(d - Z) \ , \tag{2.21}$$

where

$$d = \omega_0/\ell\beta \ ,$$

and ℓ is the X-component of $\underset{\sim}{\kappa}_H$; the solution of (2.16) gives n as a function of Z only, determined from (2.2),

$$|n| = \kappa_H\left(\frac{N^2}{\omega^{*2}} - 1\right)^{\frac{1}{2}} \ . \tag{2.22}$$

The sign of n is chosen to determine the direction of propagation of the wave packet (from (2.19), for upward propagation, the product $n\omega^*$

must be negative). The path of the wave packet is given by

$$\left\{\frac{N^2}{\omega_0^2}\left(1-\frac{Z}{d}\right)^{-2}-1\right\}^{\frac{1}{2}}-\left\{\frac{N^2}{\omega_0^2}\left(1-\frac{\zeta}{d}\right)^{-2}-1\right\}^{\frac{1}{2}}=\pm\frac{|\ell\beta|T}{\kappa_H}\,, \qquad (2.23)$$

where ζ is the initial value of Z; a fixed value of ζ describes a particular position within the wave packet. The solution of (2.18) is

$$\mathcal{I}=\frac{\mathcal{I}_0(\zeta)W(\zeta)}{W(Z)}\exp\{-\int_{\zeta}^{Z}\frac{\lambda\kappa^2}{W}\,dZ\}\,. \qquad (2.24)$$

Here W is a function of Z only, given by (2.19), (2.21) and (2.22). $\mathcal{I}_0(\zeta)$ is the initial distribution of $\mathcal{I}$ with height. Choosing the positive sign in (2.23), this example describes propagation of a wave packet towards the critical level $Z = d(\omega^* = 0)$. As the critical level is approached

$$\left.\begin{aligned} T &\sim \left|\frac{d\kappa_0}{\omega_0 u}\right|\,, \\ \text{where}\qquad \kappa_0 &= N\kappa_H/|\omega_0|\,, \end{aligned}\right\} \qquad (2.25)$$

and

$$u=\left|1-\frac{Z}{d}\right|\,. \qquad (2.26)$$

Here κ_0 is the wavenumber at the level Z = 0. The group velocity is given by

$$|W| \sim |\omega_0 u^2/\kappa_0|\,. \qquad (2.27)$$

Thus the wave packet approaches the critical level, with a decreasing velocity, and will never reach it in finite time.

For a fixed value of ζ, as the critical level is approached the wave action $\mathcal{I}$ (given by (2.24)), will grow to a maximum value (since $W \to 0$) and will then decay rapidly to zero at a rate determined

by the dissipation parameter λ. λ is a function of Z in general, and may be expected to vary inversely with the density; however, in order to make further analytical progress, we will now assume that λ is a constant (this is not a great restriction, as it may be anticipated that dissipation will be important only in the vicinity of the critical level). For a fixed value of ζ, it follows from (2.24) that the maximum value of $\mathcal{F}$ occurs at that value of Z (or u) which satisfies

$$W_Z + \lambda\kappa^2 = 0 \ . \tag{2.28}$$

For small values of λ, this has the solution, $u = u_m$, where

$$u_m = \kappa_0 |\lambda d/2\omega_0|^{\frac{1}{3}} \{1 + \tfrac{1}{3} \kappa_H^2 |\lambda d/2\omega_0|^{\frac{2}{3}} + O(\lambda^{\frac{4}{3}})\} \ . \tag{2.29}$$

The corresponding value of the time is $T = T_m$, and is determined from (2.23):

$$T_m = |2d^2/\lambda\omega^2|^{\frac{1}{3}} \{1 - \tfrac{5}{6} \kappa_H^2 |\lambda d/2\omega_0|^{\frac{2}{3}} + O(\lambda^{\frac{4}{3}})\} - T_0 \ ,$$

where
$$T_0 = |\kappa_H d/\omega_0| \{N^2/\omega_0^2 (1 - \zeta/d)^{-2} - 1\}^{\frac{1}{2}} \ . \tag{2.30}$$

Finally, the maximum value of $\mathcal{F}$ (for fixed ζ) is found by substituting (2.29) into (2.24), and is

$$\mathcal{F}_m = \frac{\mathcal{F}_0(\zeta) W(\zeta)}{\omega_0 \kappa_0} \left|\frac{2\omega_0}{e\lambda d}\right|^{\frac{2}{3}} \{1 + \tfrac{1}{6} \kappa_H^2 |\lambda d/2\omega_0|^{\frac{2}{3}} + O(\lambda^{\frac{4}{3}})\} \ . \tag{2.31}$$

Note that u_m (the distance of the maximum from the critical level) is independent of ζ. The absolute maximum value of $\mathcal{F}$ is determined by maximising (2.32) over ζ; this absolute maximum is thus given by that value of ζ which maximises the product $\mathcal{F}_0(\zeta)W(\zeta)$; the corresponding time is determined from (2.22) by using this value of ζ to evaluate T_0.

The variation of $\mathcal{J}$ with time T is shown in Figure 1, and the variation of $\mathcal{J}_m$ with λ is shown in Figure 2.

§3. RESULTS AND DISCUSSION:

(a) Critical Layer Absorption

The equations (2.16), (2.17) and (2.18) were integrated numerically, the finite difference scheme being described in Appendix A. The equations are to be solved subject to initial conditions which specify the initial variation of $\underset{\sim}{V}$, $\mathcal{J}$ and ω (and hence n by (2.2)) with height Z. All calculations assume that N^2 is a constant, that the initial value of $\underset{\sim}{V}$ is

$$\beta Z \underset{\sim}{i} \ , \tag{3.1}$$

and that the initial value of ω is a constant, ω_0. It was found convenient to introduce new variables, m and U, where

$$m = n^{-1} \ , \tag{3.2}$$

and

$$\underset{\sim}{V} = \beta Z \underset{\sim}{i} + \underset{\sim}{\kappa}_H \, U/\rho_0 \ . \tag{3.3}$$

Note that $2\pi m$ is the vertical wavelength. Then the equations (2.16), (2.17) and (2.18) become

$$m_T - m^2 \omega_Z = 0 \ , \tag{3.4}$$

$$U_T + (\mathcal{J} W)_Z = 0 \ , \tag{3.5}$$

$$\mathcal{J}_T + (\mathcal{J} W)_Z + \lambda \kappa^2 \mathcal{J} = 0 \ . \tag{3.6}$$

Also, from (2.1) and (2.2),

$$\omega^* = \omega - \beta \ell Z - \kappa_H^2 U/\rho_0 \ , \tag{3.7}$$

$$\omega^{*2} = N^2 m^2 \kappa_H^2 / 1 + m^2 \kappa_H^2 \ , \tag{3.8}$$

$$W = -\text{sign}(m\omega^*) \, \underset{\kappa}{\cdot\cdot} \, \frac{m^2 \kappa_H^2}{(1+m^2\kappa_H^2)^{3/2}} \ . \tag{3.9}$$

Initially there is a critical level at $Z = d$, where $d = \omega_0/\ell\beta$ (2.21), and U is zero initially. The nonlinear coupling is due primarily to the last term in (3.7); indeed the ratio of $\kappa_H^2 U/\rho_0$ to ω^* provides a convenient measure of the significance of non-linear effects. Finally, we note that (3.5) and (3.6) may be combined, to give

$$U_T = \mathcal{F}_T + \lambda\kappa^2\mathcal{F} \quad . \tag{3.10}$$

The first term describes the instantaneous production of U in proportion to $\mathcal{F}$, and the second term describes the permanent formation of U due to dissipation. (3.10) also shows that U will be comparable in magnitude to $\mathcal{F}$.

For all the numerical calculations, we set $\ell = \kappa_H$, and

$$\begin{aligned} N^2 &= 0{\cdot}1 \ , \\ \omega_0 &= N/\sqrt{2} \ , \\ \kappa_H &= 0{\cdot}5 \ , \\ \beta &= 0{\cdot}05963 \ . \end{aligned} \tag{3.11}$$

For an isothermal ideal gas, it may be shown that (in our non-dimensional co-ordinates)

$$-\rho_{0Z}/\rho_0 = \frac{N^2(2\gamma-1)}{\gamma-1} \tag{3.12}$$

where γ is the ratio of the specific heats. Setting $\gamma = 1{\cdot}4$, and integrating

$$\rho_0(Z) = \exp(-0{\cdot}35Z) \ , \tag{3.13}$$

where we have chosen the scale ρ_1 so that ρ_0 (non-dimensional) is equal to one at $Z = 0$. The parameter setting (3.11) gives a

critical level at Z = 7·5, thus determining the length scale. The initial distribution of $\mathcal{F}$ is chosen to be zero outside the range $0 \leq Z \leq 2$; inside this range the initial distribution of $\mathcal{F}$ is described in the Appendix A (A.7). The initial distribution of m is determined from (3.7) and (3.8) (with U = 0 and $\omega = \omega_0$), with m negative, so that the wave packet propagates upwards and towards the critical level. If we choose a value for N_1 which corresponds to a dimensional Brunt-Väisälä frequency of $2{\cdot}1 \times 10^{-2}$ sec^{-1} (an isothermal atmosphere with the speed of sound set at 300 m/sec), then (3.11) implies an initial wave period of approximately 7 minutes. Letting $\epsilon = 0{\cdot}1$ say, the length scale L_1 is approximately 230 m, which (with $\kappa_H = 0{\cdot}5$) leads to a horizontal wavelength of approximately 3 km. The initial values of $\mathcal{F}$ are varied over the range 10^{-2} to 10^{-5}; with N_1, L_1 as above, an initial value of $\mathcal{F}$ equal to 10^{-3} corresponds to a vertical particle velocity of approximately 0·15 m/sec. The dissipation parameter λ is assumed to be a constant, which is varied over the range 0 to 10^{-5}; a value of 10^{-3}, with ϵ, N_1, L_1 as above, gives E, the inverse Reynolds number, as about 10^{-2}, and a kinematic viscosity of about 11 $m^2 sec^{-1}$. The parameter setting (3.11) with $\lambda = 10^{-3}$ implies that T_m for the small amplitude case is 108·6; this time scale is also appropriate for the nonlinear equations.

First the equations were integrated numerically in the small amplitude limit (U set equal to zero, and (3.5) ignored). Figure 1, for which λ is 10^{-3}, shows the variation of the wave packet with time as it propagates towards the critical level. The wave packet narrows and increases in magnitude until it reaches its maximum $\mathcal{F}_m$, after which it is strongly dissipated and decays rapidly to

zero. The numerical results agreed with the theoretical results (2.29), (2.30) and (2.31); for instance, with λ set at 10^{-3}, the numerical results gave $\mathcal{F}_m / \mathcal{F}_{0m} = 9{\cdot}00$ ($\mathcal{F}_{0m}$ is the maximum value of $\mathcal{F}$ at T = 0), at $Z_m = 6{\cdot}08$ and $T_m = 102{\cdot}7$, while the theoretical results are $\mathcal{F}_m / \mathcal{F}_{0m} = 9{\cdot}53$, at $Z_m = 6{\cdot}13$ and $T_m = 108{\cdot}6$. Also shown in Figure 1 is the result of allowing λ to vary inversely with the density i.e. $\lambda = \lambda_0 \exp(0{\cdot}35Z)$ with λ_0 chosen so that λ is 10^{-3} at $Z = 6{\cdot}13$. The variation of the wave packet in time is similar to that when λ is a constant, although the wave packet is narrower and reaches a larger maximum ($\mathcal{F}_m / \mathcal{F}_{0m} = 10{\cdot}13$ at $Z_m = 6{\cdot}11$ and $T_m = 105{\cdot}5$). Figure 2 shows the computed values of $\mathcal{F}_m / \mathcal{F}_{0m}$ as a function of λ in comparison with the theoretical result (obtained from (2.31)); the drift away from the theoretical value as λ decreases is a consequence of the number of grid points (the same for all results shown), and may be corrected by increasing the number of grid points.

Next the fully nonlinear equations (3.4) to (3.9) were integrated with the parameter setting (3.11). Two parameters were available to vary, the dissipation parameter λ, and the magnitude of the wave packet at T = 0, measured by $\mathcal{F}_{0m}$ (the maximum value of $\mathcal{F}$ at T = 0). With $\mathcal{F}_{0m}$ set at 10^{-7}, the results were virtually indistinguishable from the small amplitude case; with $\lambda = 10^{-3}$, there was a difference of less than 1% in $\mathcal{F}_m / \mathcal{F}_{0m}$, Z_m and T_m; also m varied by less than 4% from its initial value, which may be compared with the small amplitude case in which m does not change with time. As $\mathcal{F}_{0m}$ is increased, so does the extent of the interaction with the mean wind; an indication of this is contained in Figure 2, which

shows the variation of $\mathcal{F}_m / \mathcal{F}_{0m}$ with λ for $\mathcal{F}_{0m} = 10^{-5}$, and 10^{-3}, compared with the corresponding results for the small amplitude case. Figure 3 shows the variation of $\mathcal{F}$ with time, for different values of $\mathcal{F}_{0m}$ and λ set at 10^{-3}; as $\mathcal{F}_{0m}$ is increased the ratio $\mathcal{F}_m / \mathcal{F}_{0m}$ decreases, and the wave packet reaches its maximum earlier in time and at a lower level of Z; for example,

$$\begin{aligned} &\text{if } \mathcal{F}_{0m} = 10^{-5}, \quad \mathcal{F}_m / \mathcal{F}_{0m} = 6{\cdot}90, \quad Z_m = 5{\cdot}80, \quad T_m = 81{\cdot}7, \\ &\text{if } \mathcal{F}_{0m} = 10^{-3}, \quad \mathcal{F}_m / \mathcal{F}_{0m} = 2{\cdot}37, \quad Z_m = 4{\cdot}17, \quad T_m = 29{\cdot}7. \end{aligned} \tag{3.14}$$

By contrast with the small amplitude, or no interaction, case the wave packet remains broader, achieves a lower maximum and does not decay so rapidly after its maximum has been reached. For the larger values of $\mathcal{F}_{0m}$ (10^{-2} and 10^{-3}), a significant part of the interaction with the mean wind has occurred some distance from the critical level. An interesting feature is that after the maximum $\mathcal{F}_m$ has been achieved, the shape of the wave packet changes and two subsidiary peaks develop at each end; this is clearly so because the interaction with the mean wind is correlated with the gradient $(\mathcal{F}W)_Z$, as well as with $\mathcal{F}_{0m}$, and these gradients are largest at the ends of the wave packet. Figure 5 shows the variation of $\mathcal{F}$ with time, for different values of λ with $\mathcal{F}_{0m}$ set at 10^{-3}; also shown is the case when λ is not a constant but varies inversely with the density i.e. $\lambda = \lambda_0 \exp(0{\cdot}35Z)$ with λ_0 chosen so that λ is 10^{-3} at $Z = 6{\cdot}13$.

The corresponding variation of U with time is shown in Figure 4 ($\lambda = 10^{-3}$, and different values of $\mathcal{F}_{0m}$) and Figure 6 ($\mathcal{F}_{0m} = 10^{-3}$, and different values of λ). Generally the behaviour of U with

time follows the same pattern as $\mathcal{F}$ with two significant differences. Firstly, the values of U are slightly larger than those of $\mathcal{F}$; for example, if U_m is defined to be the maximum value of U (achieved at a height Z_m and time T_m as in (3.14))

$$\text{if } \mathcal{F}_{0m} = 10^{-5}, \quad U_m/\mathcal{F}_{0m} = 7{\cdot}22 ,$$
$$\text{if } \mathcal{F}_{0m} = 10^{-3}, \quad U_m/\mathcal{F}_{0m} = 2{\cdot}40 . \tag{3.15}$$

Secondly after the wave packet has passed (and $\mathcal{F}$ reverts to zero), there is a residual nonzero value of U. It is clear from (3.10) that both these effects are due to dissipation. A term $-\mathcal{F}_0(Z)$ has been subtracted from U in Figures 4 and 6; this term is due to the impulsive nature of the initial value problem posed for (3.4) to (3.9), and is physically unimportant; if the wave packet is generated by a continuous forcing at the level Z = 0 this term would not have arisen. The relationship between U and the mean wind $\underset{\sim}{V}$ is described by (3.3); if V_M denotes the difference between $|\underset{\sim}{V}|$ and its initial value βZ (3.1), then

$$V_M = \kappa_H U/\rho_0 . \tag{3.16}$$

Here κ_H (3.11) is a constant, but $\rho_0(Z)$ (3.13) decreases with height. Figure 7 shows V_M at times when it is close to its maximum for $\lambda = 10^{-3}$ and $\mathcal{F}_{0m} = 10^{-2}, 10^{-3}$; also shown for comparison is the initial value of $|\underset{\sim}{V}|$ (3.1).

Instead of the initial value problem considered so far, an alternative method of generating a wave packet is to set $\mathcal{F}$ equal to zero at T = 0 for $0 < Z \leq 10$, and impose a forcing term at Z = 0 for T > 0 by specifying $\mathcal{F}(T,0)$; here, we simply imposed the condition that

$\mathcal{F}(T,0) = \mathcal{F}_{0m}$ (a constant). This procedure is analogous to that used by Jones and Houghton (1971) and Breeding (1971). In the small amplitude case, a steady state is achieved after the arrival of the front of the wave packet and $\mathcal{F}$ is then given by (2.24) but now $\zeta = 0$, and $\mathcal{F}_0(\zeta)$ is the constant $\mathcal{F}_{0m}$. The maximum $\mathcal{F}_m$ is reached for times $T > 112{\cdot}4$ and $\mathcal{F}_m/\mathcal{F}_{0m}$ is $11{\cdot}11$ at the height $Z_m = 6{\cdot}13$. The results for the nonlinear equations are shown in Figure 8 (with $\mathcal{F}_{0m} = 10^{-3}$ and $\lambda = 10^{-3}$). $\mathcal{F}/\mathcal{F}_{0m}$ now increases up to a maximum of approximately 10 at around $Z = 5{\cdot}2$, and for times $T > 110$ oscillates slightly about this value. However U continues to increase and for times $T > 150$ an instability in the finite difference scheme occurs, when $m\kappa_H$ exceeds $\sqrt{2}$ and the stability criterion (A.5) no longer applies.

(b) The "Self-Destructing" Wave

The system of equations was also integrated numerically for the case when there was no initial region of wind shear, and the mean wind was initially zero. There is then no critical level but the wave packet still generates a mean wind which extracts energy from the wave packet. This case is obtained by putting $\beta = 0$ in (3.3) and (3.7), the remaining equations (3.4) to (3.9) being unchanged. The parameter setting was

$$\begin{aligned} N^2 &= 0{\cdot}1 \ , \\ \omega_0 &= N\sqrt{2}/5 \ , \\ \kappa_H &= 0{\cdot}5 \ , \\ \beta &= 0 \ . \end{aligned} \qquad (3.17)$$

$\rho_0(Z)$ is given by (3.13). The value for ω_0 was selected to ensure that the wave packet (given initially by (A.7) as in (a)) remains in the

range $0 < Z < 10$ for sufficient time for significant interaction to occur.

In the small amplitude limit the theoretical result (2.24) shows that the wave packet propagates vertically upwards at a constant speed and without change of shape except for a slow exponential decay due to dissipation; with λ set at 10^{-3}, this decay was negligible for $0 \leq Z \leq 10$. Figures 9, 10 show the results for the nonlinear equations. With $\lambda = 0$, U is identically equal to $\mathcal{F}$, but now $\mathcal{F}$ decays with height and the wave packet propagates vertically at a slower speed. For an initial magnitude $\mathcal{F}_{0m} = 10^{-2}$, at $T = 100$, the wave packet has reached $Z = 4{\cdot}0$ (in the small amplitude limit the corresponding height is $Z = 5{\cdot}9$), and has decayed to one-half of its initial magnitude; in this case there is a small initial increase in $\mathcal{F}$, and the wave packet broadens considerably in an asymmetrical manner, the maximum occurring at the lower end. For an initial magnitude $\mathcal{F}_{0m} = 10^{-3}$, at $T = 100$, the wave packet has reached $Z = 5{\cdot}6$ and has decayed to $0{\cdot}85$ of its initial magnitude; the broadening of the wave packet is not so noticeable. With $\lambda = 10^{-3}$, the results followed a similar pattern, but due to the effects of dissipation U is larger than $\mathcal{F}$, and there is a residual value of U after the passage of the wave packet. For $\mathcal{F}_{0m} = 10^{-2}$, at $T = 100$ the wave packet has reached $Z = 4{\cdot}1$ and has decayed to $0{\cdot}34$ of its initial magnitude, while $U/\mathcal{F}_{0m}$ is $0{\cdot}44$ and the residual value of U is a constant $0{\cdot}11 \times 10^{-2}$. For $\mathcal{F}_{0m} = 10^{-3}$, at $T = 100$, the wave packet has reached $Z = 5{\cdot}7$ and has decayed to $0{\cdot}63$ of its initial magnitude, while $U/\mathcal{F}_{0m}$ is $0{\cdot}67$ and the residual value of U is a constant $0{\cdot}09 \times 10^{-3}$. Figure 11 shows the actual mean wind V_M generated (3.16) at $T = 50, 100$ for $\lambda = 0, 10^{-3}$ and $\mathcal{F}_{0m} = 10^{-2}$.

Figure 12 shows the results of continuously generating the wave packet at Z = 0, by prescribing $\mathcal{F} = \mathcal{F}_{0m}$ there (and setting $\mathcal{F} = 0$ for T = 0 and $0 < Z \leq 10$). In the small amplitude limit the front of the wave packet so generated propagates vertically at a constant speed, and $\mathcal{F}$ is constant behind the front, apart from a negligibly small exponential decay due to dissipation. In the nonlinear case, with $\mathcal{F}_{0m} = 10^{-2}$, and $\lambda = 0$, U is identically equal to $\mathcal{F}$, but the front of the wave packet is broader and propagates at a slower speed; behind the front there is a small increase in the value of $\mathcal{F}$ e.g. the maximum value of $\mathcal{F}/\mathcal{F}_{0m}$ at T = 100 is 1·17. With $\lambda = 10^{-3}$ and $\mathcal{F}_{0m} = 10^{-2}$, the results are similar, but there is a smaller increase in $\mathcal{F}$ and due to the effects of dissipation U is larger than $\mathcal{F}$ e.g. at T = 100 the maximum value of $U/\mathcal{F}_{0m}$ is 1·42.

The author gratefully acknowledges the assistance of Mr. D.J. Beaumont and Mr. R. Hesline, who prepared and executed the computer programme. This research was supported by A.R.G.C. Grant, No. G73/15040.

APPENDIX A: THE FINITE DIFFERENCE SCHEME

The equations that were integrated numerically are (3.4) to (3.9); they may be written in the form

$$\underline{u}_T + A\underline{f}_Z + \underline{b} = \underline{0} \qquad (A.1)$$

where $$\underline{u} = \begin{bmatrix} m \\ U \\ \mathcal{J} \end{bmatrix}, \quad \underline{f} = \begin{bmatrix} \omega \\ \mathcal{J}W \\ \mathcal{J}W \end{bmatrix}, \quad \underline{b} = \begin{bmatrix} 0 \\ 0 \\ \lambda\kappa^2 \end{bmatrix},$$

and $$A = \begin{bmatrix} -m^2 & 0 & 0 \\ 0 & 1 & 0 \\ 0 & 0 & 1 \end{bmatrix} . \qquad (A.2)$$

Here ω, W are known functions of m, U, $\mathcal{J}$ (and also explicitly of Z) by virtue of (3.7), (3.8) and (3.9); κ^2 is equal to $m^{-2}(1 + m^2\kappa_H^2)$, and λ is a known function of Z. This system of equations is hyperbolic, provided that $m^2\kappa_H^2 < 2$, and the characteristic directions are given by

$$\frac{dZ}{dT} = 0, \quad W \pm (-m^2\kappa_H^2 W_m \mathcal{J}/\rho_0)^{\frac{1}{2}} . \qquad (A.3)$$

Here W_m is the explicit derivative of W with respect to m, and is

$$W_m = Nm\kappa_H(2 - m^2\kappa_H^2)(1 + m^2\kappa_H^2)^{-\frac{5}{2}} . \qquad (A.4)$$

Since $\mathcal{J}$ is just the energy density divided by ω^*, $\mathcal{J}$ has the same sign as ω^* and hence the opposite sign to m; thus the square root in (A.3) will lead to a real characteristic direction when $m^2\kappa_H^2 < 2$. Near the critical level, m tends to zero, and hence the choice of a finite difference scheme to approximate (A.1) is based on the assumption that the system (A.1) is hyperbolic.

Two explicit finite difference schemes were investigated. The first employed a forward difference for the T-derivative in (A.1), and a backward difference for the Z-derivative in (A.1). Thus the system of equations is approximated by, at the grid point (Z,T),

$$\underset{\sim}{u}(T + \Delta T,Z) = \underset{\sim}{u}(T,Z) - A(T,Z)\,\frac{\Delta T}{\Delta Z}\,(\underset{\sim}{f}(T,Z) - \underset{\sim}{f}(T,Z - \Delta Z)) - \Delta T\underset{\sim}{b}(T,Z)\ . \qquad (A.4)$$

Starting with the initial data $\underset{\sim}{u}(0,Z)$, (A.4) enables $\underset{\sim}{u}(T + \Delta T,Z)$ to be calculated from $\underset{\sim}{u}(T,Z)$ at a set of grid points in the range $0 \leq Z \leq 10$. As the wave packet propagates upwards, $\underset{\sim}{u}(T,0)$ was maintained at its initial value; also $\underset{\sim}{u}(T,10)$ was maintained at its initial value, as the critical level is at $Z = 7.5$, and there is no wave penetration above this level. This scheme is first order in accuracy. In order to obtain an indication of the stability of (A.4), the scheme was linearised about the local value of $\underset{\sim}{u}(T,Z)$ and the von Neumann necessary condition for stability (Richtmeyer and Morton, 1967) then applied. The result was

$$\frac{\Delta T}{\Delta Z}\,\{W \pm (-m^2\kappa_H^2 W_m \mathcal{F}/\rho_0)^{\frac{1}{2}}\} \leq 1\ . \qquad (A.5)$$

This result can also be deduced from the Courant-Friedrichs-Lewy criterion that the ratio $\Delta T/\Delta Z$ should be less than the reciprocal of the maximum characteristic speed.

The finite difference scheme (A.4) was found to be adequate for all the calculations attempted. However, as the wave packet propagates towards the critical level, it narrows and peaks simultaneously (see Figure 1) and thus generates large gradients in $\mathcal{F}$ and U; hence a large number of grid points are needed to resolve these gradients, and

from (A.5), there is a consequent reduction in the permissible time step. In order to reduce the computer time, another finite difference scheme, of second order accuracy, was tried. This was the "leapfrog" scheme, in which both T- and Z-derivatives in (A.1) are approximated by central differences:

$$\underset{\sim}{u}(T + \Delta T,Z) = \underset{\sim}{u}(T - \Delta T,Z) - A(T,Z)\,\frac{\Delta T}{\Delta Z}\,(\underset{\sim}{f}(T,Z + \Delta Z) - \underset{\sim}{f}(T,Z - \Delta Z)) - 2\Delta T\underset{\sim}{b}(T,Z)\ . \qquad (A.6)$$

The scheme is integrated forward in time in a manner analogous to that described above for (A.4), but now the data values of $\underset{\sim}{u}(T,Z)$ must be stored at two time levels. The von Neumann necessary condition for stability shows that (A.6) is neutrally stable if (A.5) is satisfied.

The numerical results of §3 were mostly obtained using as initial data for $\mathcal{J}$:

$$\mathcal{J}_0 = \begin{cases} \mathcal{J}_{0m}\exp\{1 - (Z(2-Z))^{-\frac{1}{2}}\}, & 0 \leq Z \leq 2, \\ 0 & Z > 2. \end{cases} \qquad (A.7)$$

A variety of other, similar, bell-like shapes were also investigated. However, qualitatively, the results appeared to be independent of the precise form used; indeed, a square-wave ($\mathcal{J} = \mathcal{J}_{0m}$, $0 \leq Z \leq 2$ and 0, $Z > 2$) gave results very close to those obtained from (A.7). An alternative to prescribing the initial values of $\mathcal{J}$ is to generate the wave packet by prescribing $\mathcal{J}$ at the level $Z = 0$. As the wave packet propagates vertically upwards, it narrows and peaks, generating large gradients. However, at any one time, the wave packet occupies only a small portion of the Z-grid. Hence two sets of grid points were used;

a fixed coarse grid from $0 \leq Z \leq 10$, and a fine, floating grid which moved with the wave packet. This fine grid was determined by the requirement that it occupy the region where $\mathcal{F} > \mathcal{F}_{0m}10^{-3}$, plus a region extending a further 20% upwards. When the wave packet reached the top of the fine grid, this would be reset. This resetting of the fine grid necessitated the calculating of the data values of $\underset{\sim}{u}(T,Z)$ at the new grid points by interpolation from the old grid points; a four-point interpolation formula was used (several different interpolation formulae were tried, and made little perceptible difference). As the "leapfrog" scheme assumes that ΔZ is constant throughout the grid, it cannot be used at the ends of the fine grid; at these grid points (A.4) was used instead. The stability criterion (A.5) was applied whenever the fine grid was reset, to determine the new time step; this enabled us to take advantage of the fact that generally W decreases as the wave propagates vertically. ΔT was initially set at 0.2.

Both finite difference schemes were tested in the small amplitude limit (setting $U \equiv 0$ in (A.1) and neglecting the second equation), as the numerical results may then be compared with the theoretical results ((2.29), (2.30) and (2.31)). Using the "leapfrog" scheme, and 300 grid points on the fine grid, agreement to within 2½% was obtained, with λ set at 10^{-3}. Using only 200 grid points on the fine grid, and the "leapfrog" scheme, gave agreement to within 5%; comparable agreement with (A.4) required 300 grid points. For the fully non-linear system similar indications of convergence were obtained. However, smaller values of λ required a greater number of points in the fine grid to obtain comparable accuracy. (Figure 2, for the small amplitude limit, gives an

indication of the variation of the accuracy with λ, for 200 points on the fine grid.) All the results shown have 200 points across the fine grid. When (A.5) is satisfied, the scheme (A.4) was found to be stable; however, the "leapfrog" scheme occasionally developed spurious oscillations (usually at the edges of the fine grid). Most of the results shown were obtained with the "leapfrog" scheme; however, when this scheme showed signs of instability, the results were supplemented by using (A.4). Also, for the larger values of $\mathcal{J}_{0m}$ and λ, the scheme (A.4) was completely adequate, as large gradients did not develop. All the numerical results were obtained on the CDC CYBER 73 at the University of Melbourne.

REFERENCES

Booker, J.R. and Bretherton, F.P., 1967, J. Fluid Mech. *27*, 513-539.

Breeding, R.J., 1971, J. Fluid Mech. *50*, 545-563.

Breeding, R.J., 1972, J. Geophys. Res. *77*, 2681-2692.

Bretherton, F.P. and Garrett, C.J.R., 1969, Proc. Roy. Soc. *302A*, 529-554.

Gossard, E.E., Richter, J.H. and Atlas, D., 1970, J. Geophys. Res. *75*, 3523-3536.

Grimshaw, R., 1972, J. Fluid Mech. *54*, 193-207.

Grimshaw, R., 1974, Geophys. Fluid Dynamics (to be published).

Grimshaw, R., 1975, J. Fluid Mech. (submitted for publication).

Hines, C.O., 1972, Nature *239*, 73-78.

Hines, C.O. and Reddy, C.A., 1967, J. Geophys. Res. *72*, 1015-1034.

Jones, W.L. and Houghton, D.D., 1971, J. Atmos. Sci. *28*, 604-608.

Jones, W.L. and Houghton, D.D., 1972, J. Atmos. Sci. *29*, 844-849.

Lindzen, R.S. and Holton, J.R., 1968, J. Atmos. Sci. *25*, 1095-1107.

Richtmeyer, R.D. and Morton, K.W., 1967, *Difference Methods for Initial-Value Problems*, 2nd Ed., Interscience.

FIGURE CAPTIONS

Figure 1: (β = ·05963) The graph of $\mathcal{F}/\mathcal{F}_{0m}$ against Z in the small amplitude limit, at the successive times T = 0, 20, 40, 60, 80, 100 and 120; (a) The dissipation parameter $\lambda = 10^{-3}$. (b) The dissipation parameter λ varies inversely with the density, $\lambda = 0{\cdot}1173 \times 10^{-3} \exp(0{\cdot}35Z)$.

Figure 2: (β = ·05963) The graph of $\mathcal{F}_m/\mathcal{F}_{0m}$ against the dissipation parameter λ, both plotted on a logarithmic scale; ——— the theoretical value for the small amplitude limit, · the computed value for the small amplitude limit, x the computed value for $\mathcal{F}_{0m} = 10^{-5}$, ⊙ the computed value for $\mathcal{F}_{0m} = 10^{-3}$.

Figure 3: (β = ·05963) The graph of $\mathcal{F}/\mathcal{F}_{0m}$ against Z, for $\lambda = 10^{-3}$, at the successive times T = 0, 20, 40, 60, 80 and 100; (a) $\mathcal{F}_{0m} = 10^{-5}$; (b) $\mathcal{F}_{0m} = 10^{-4}$; (c) $\mathcal{F}_{0m} = 10^{-3}$ (T = 80 is not shown); (d) $\mathcal{F}_{0m} = 10^{-2}$ (T = 60, 100 are not shown).

Figure 4: (β = ·05963) The graph of $U/\mathcal{F}_{0m}$ against Z, for $\lambda = 10^{-3}$, at the successive times T = 20, 40, 60, 80 and 100; (a) $\mathcal{F}_{0m} = 10^{-5}$; (b) $\mathcal{F}_{0m} = 10^{-4}$; (c) $\mathcal{F}_{0m} = 10^{-3}$ (T = 80 is not shown); (d) $\mathcal{F}_{0m} = 10^{-2}$ (T = 60, 100 are not shown). - - - - The residual value of U (time independent after the passage of the wave packet).

Figure 5: (β = ·05963) The graph of $\mathcal{F}/\mathcal{F}_{0m}$ against Z, for $\mathcal{F}_{0m} = 10^{-3}$, at the successive times T = 0, 20, 40, 60, 100; (a) $\lambda = 10^{-4}$; (b) $\lambda = 10^{-3}$; (c) $\lambda = 0{\cdot}1173 \times 10^{-3} \exp(0{\cdot}35Z)$; (d) $\lambda = 10^{-2}$ (T = 100 is not shown as $\mathcal{F}/\mathcal{F}_{0m} < {\cdot}02$).

Figure 6: (β = ·05963) The graph of $U/\mathcal{F}_{0m}$ against Z, for $\mathcal{F}_{0m} = 10^{-3}$, at the successive times T = 20, 40, 60, 100; (a) $\lambda = 10^{-4}$;

(b) $\lambda = 10^{-3}$; (c) $\lambda = 0{\cdot}1173 \times 10^{-3} \exp(0{\cdot}357)$; (d) $\lambda = 10^{-2}$. - - - - The residual value of U (time independent after the passage of the wave packet).

Figure 7: ($\beta = {\cdot}05963$) The graph of V_M against Z for $\lambda = 10^{-3}$; (a) $\mathcal{F}_{0m} = 10^{-2}$, T = 20, 40, 80; (b) $\mathcal{F}_{0m} = 10^{-3}$, T = 40, 60, 100.

Figure 8: ($\beta = {\cdot}05963$) The wave packet generated continuously at Z = 0 for $\mathcal{F}_{0m} = 10^{-3}$, $\lambda = 10^{-3}$; (a) $\mathcal{F}/\mathcal{F}_{0m}$ against Z; (b) $U/\mathcal{F}_{0m}$ against Z; both graphs drawn at the successive times T = 20, 60, 100.

Figure 9 ($\beta = 0$): The graph of $\mathcal{F}/\mathcal{F}_{0m}$ against Z at the successive times T = 0, 40, 60, 80, 100; (a) $\lambda = 0$, $\mathcal{F}_{0m} = 10^{-2}$; (b) $\lambda = 0$, $\mathcal{F}_{0m} = 10^{-3}$; (c) $\lambda = 10^{-3}$, $\mathcal{F}_{0m} = 10^{-2}$; (d) $\lambda = 10^{-3}$, $\mathcal{F}_{0m} = 10^{-3}$.

Figure 10 ($\beta = 0$): The graph of $U/\mathcal{F}_{0m}$ against Z at the successive times T = 40, 60, 80, 100; (a) $\lambda = 0$, $\mathcal{F}_{0m} = 10^{-2}$; (b) $\lambda = 0$, $\mathcal{F}_{0m} = 10^{-3}$; (c) $\lambda = 10^{-3}$, $\mathcal{F}_{0m} = 10^{-2}$; (d) $\lambda = 10^{-3}$, $\mathcal{F}_{0m} = 10^{-3}$. - - - - The residual value of U (time independent after the passage of the wave packet).

Figure 11 ($\beta = 0$): The graph of V_M against Z for $\mathcal{F}_{0m} = 10^{-2}$ at the successive times T = 40, 60, 80, 100; (a) $\lambda = 0$; (b) $\lambda = 10^{-3}$.

Figure 12 ($\beta = 0$): The wave packet generated continouusly at Z = 0 for $\mathcal{F}_{0m} = 10^{-2}$, $\lambda = 10^{-3}$; (a) $\mathcal{F}/\mathcal{F}_{0m}$ against Z; (b) $U/\mathcal{F}_{0m}$ against Z; both graphs drawn at the successive times T = 20, 60, 100.

Figure 1

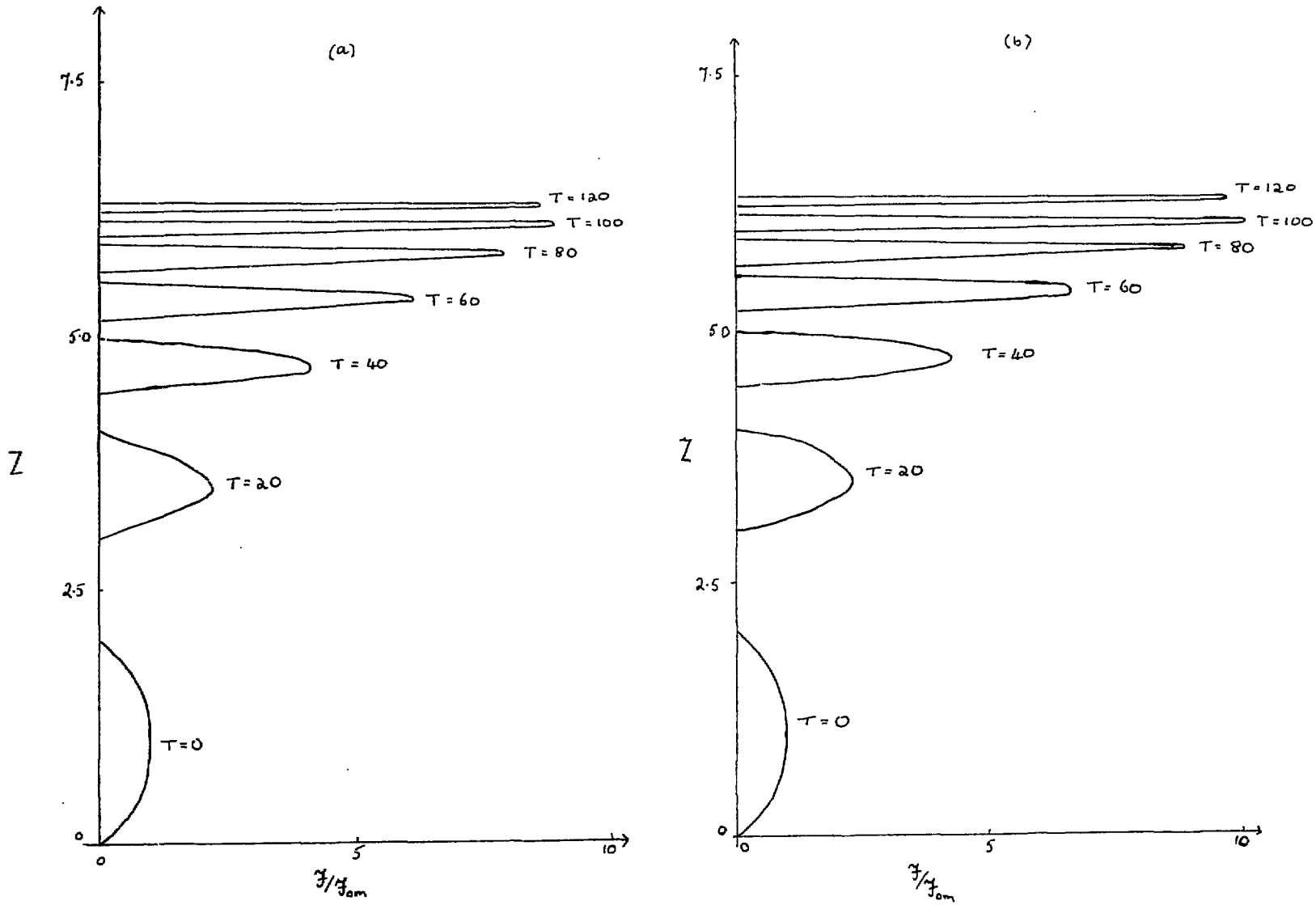
(a)
7.5
5.0
2.5
0
Z
T = 120
T = 100
T = 80
T = 60
T = 40
T = 20
T = 0
0
5
10
$\mathcal{F}/\mathcal{F}_{am}$
(b)
7.5
5.0
2.5
0
Z
T = 120
T = 100
T = 80
T = 60
T = 40
T = 20
T = 0
0
5
10
$\mathcal{F}/\mathcal{F}_{am}$

Figure 2

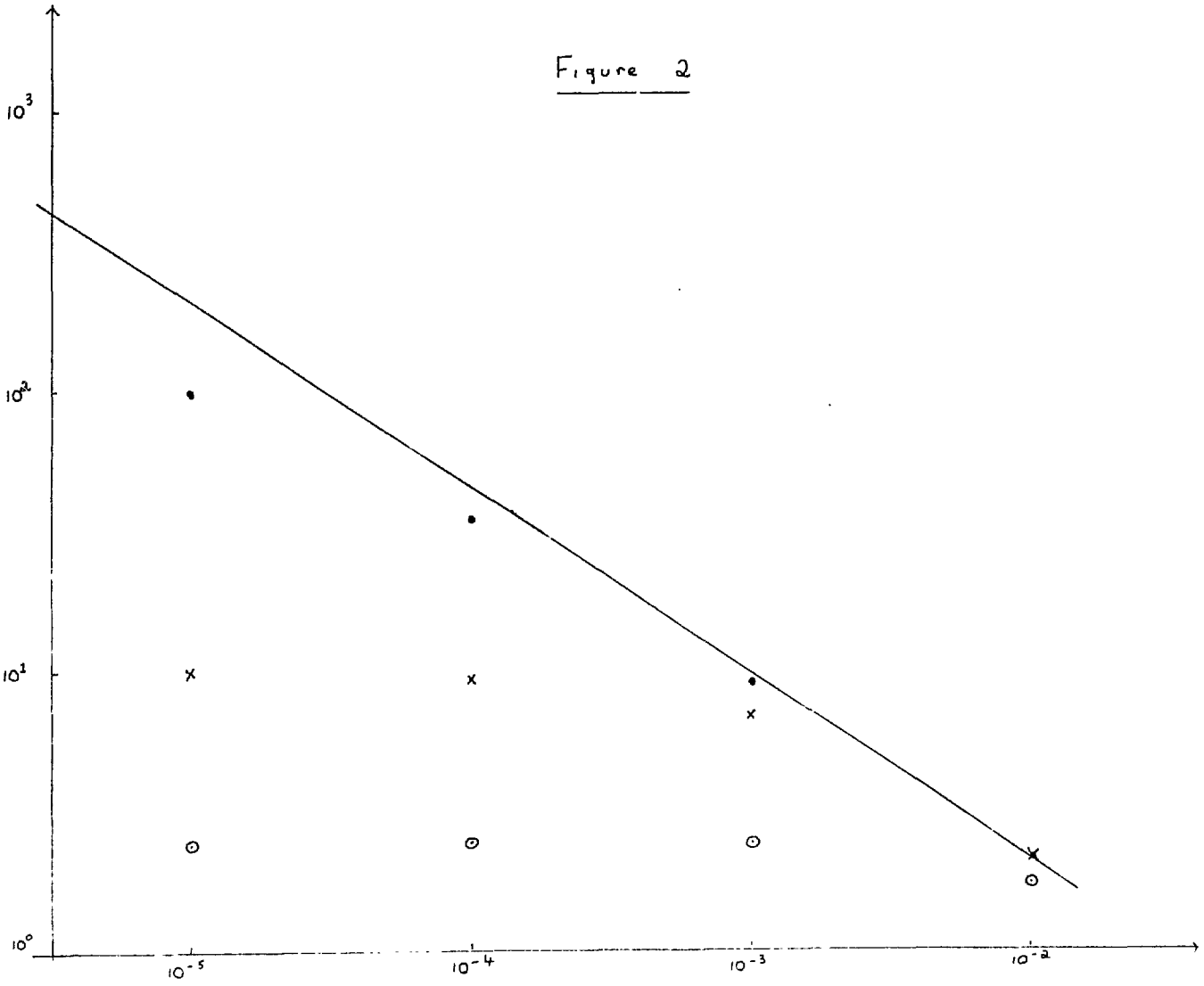

Figure 3

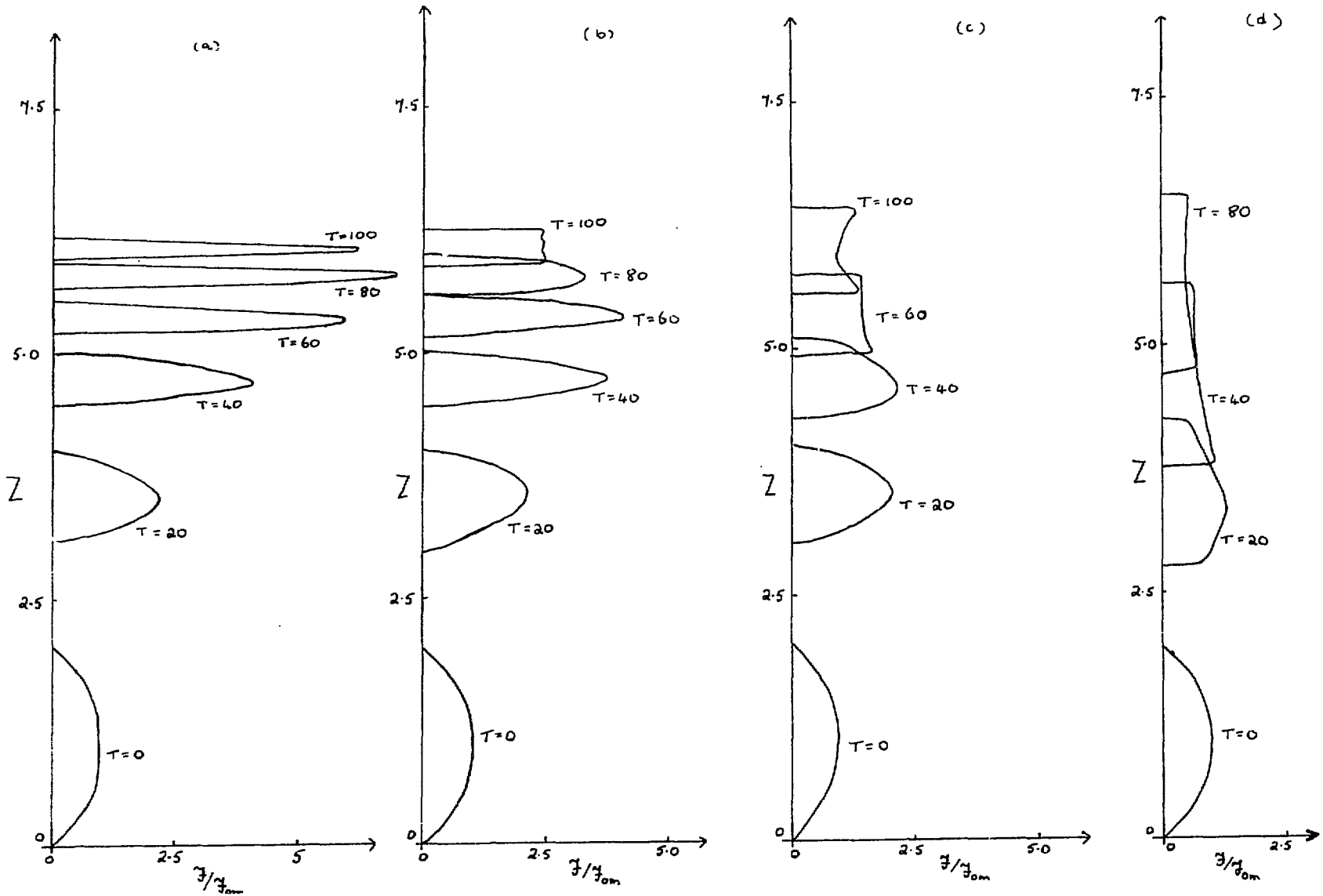
(a)
(b)
(c)
(d)
7·5
5·0
2·5
0
Z
T=100
T=80
T=60
T=40
T=20
T=0
2·5
5
5·0
$\mathcal{F}/\mathcal{F}_{om}$

Figure 4

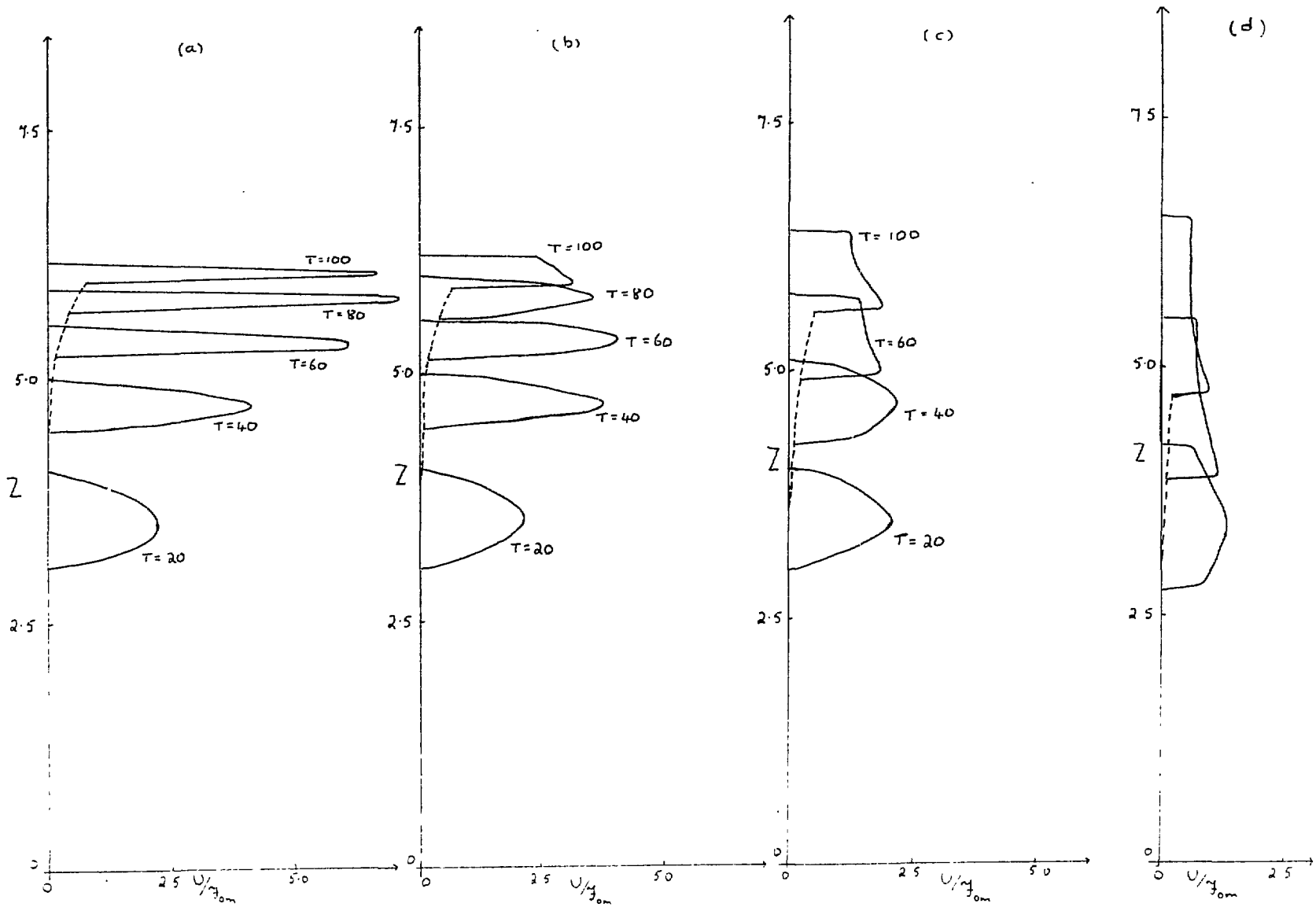

Figure 5

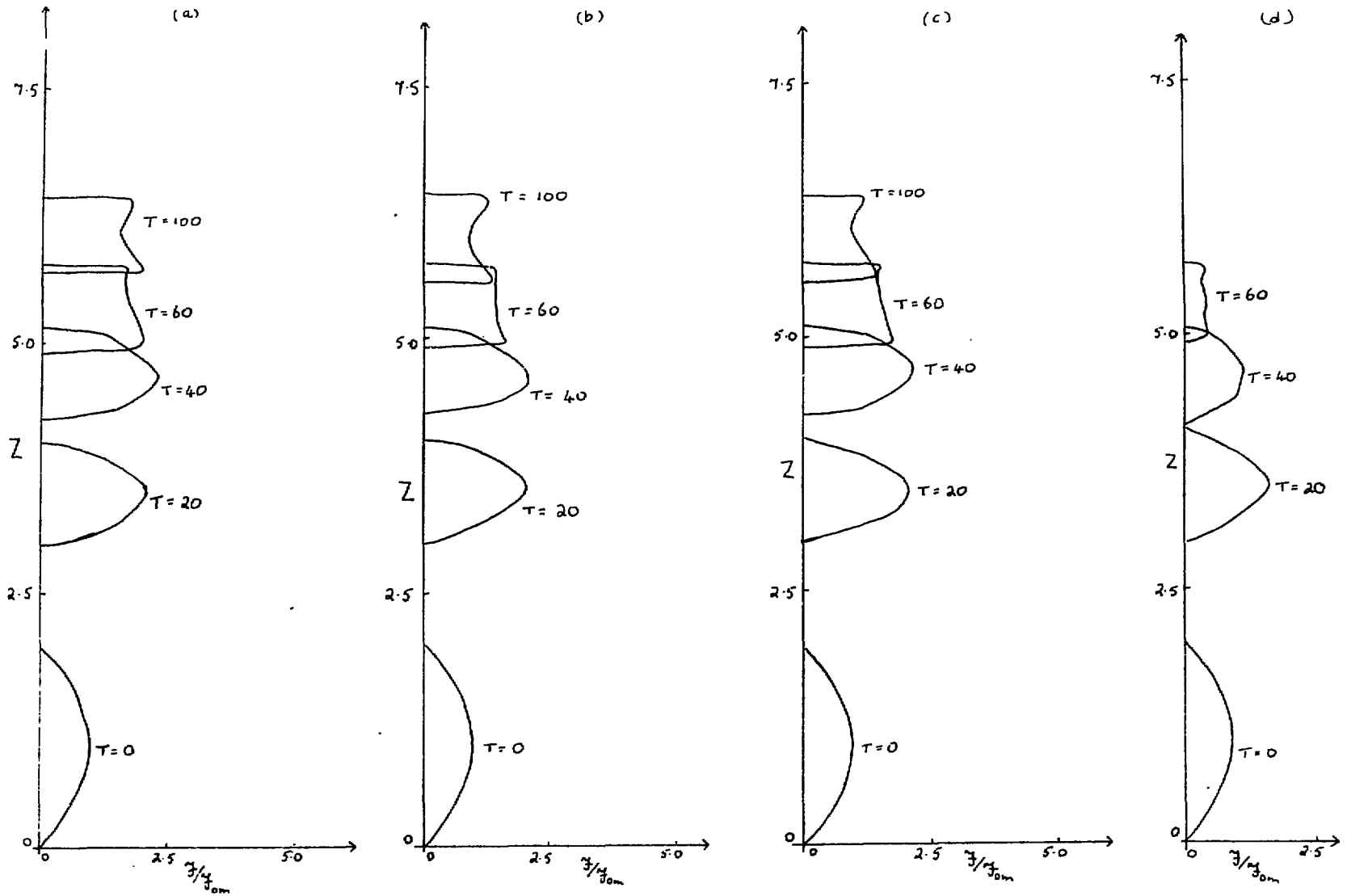

Figure 6

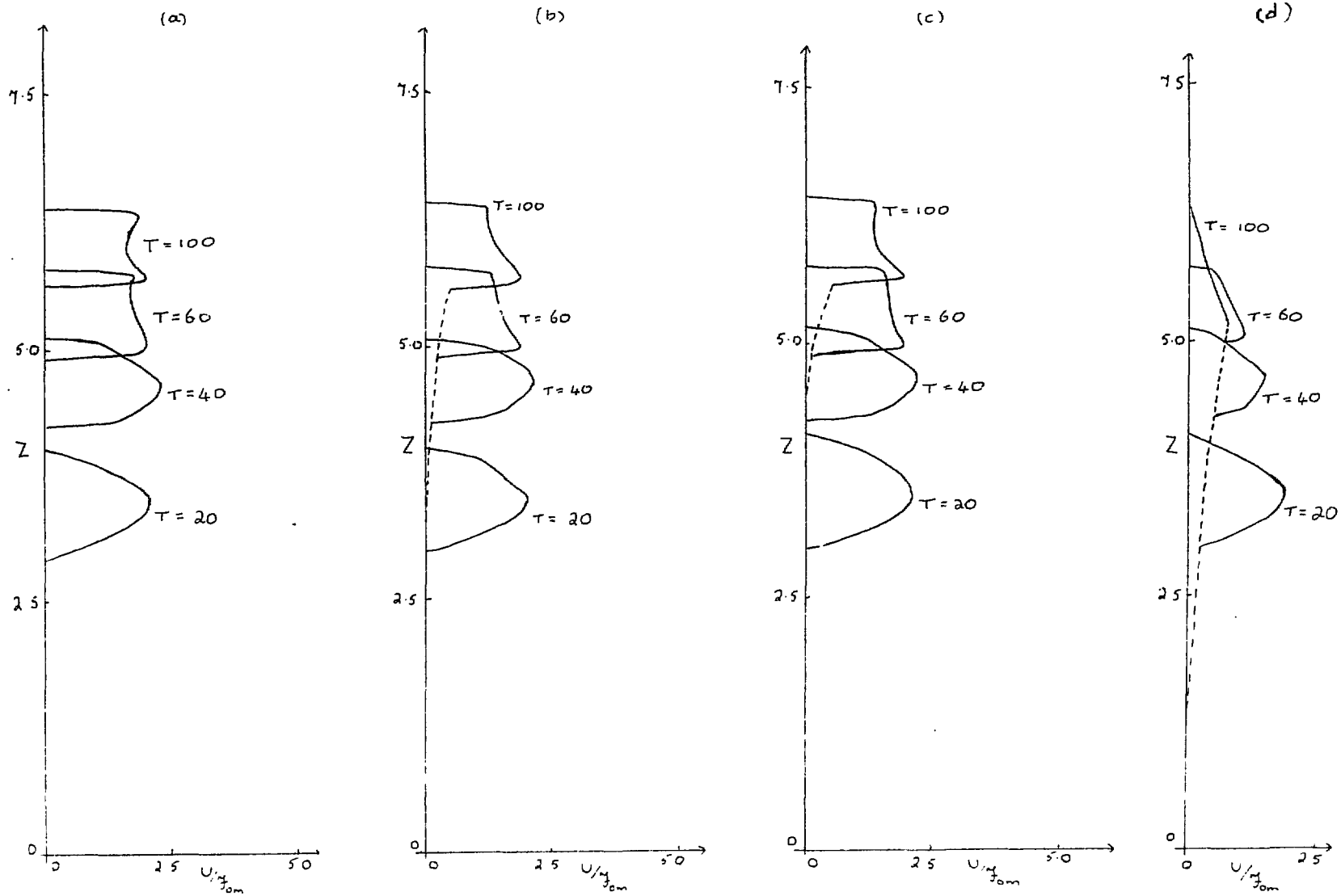

Figure 7

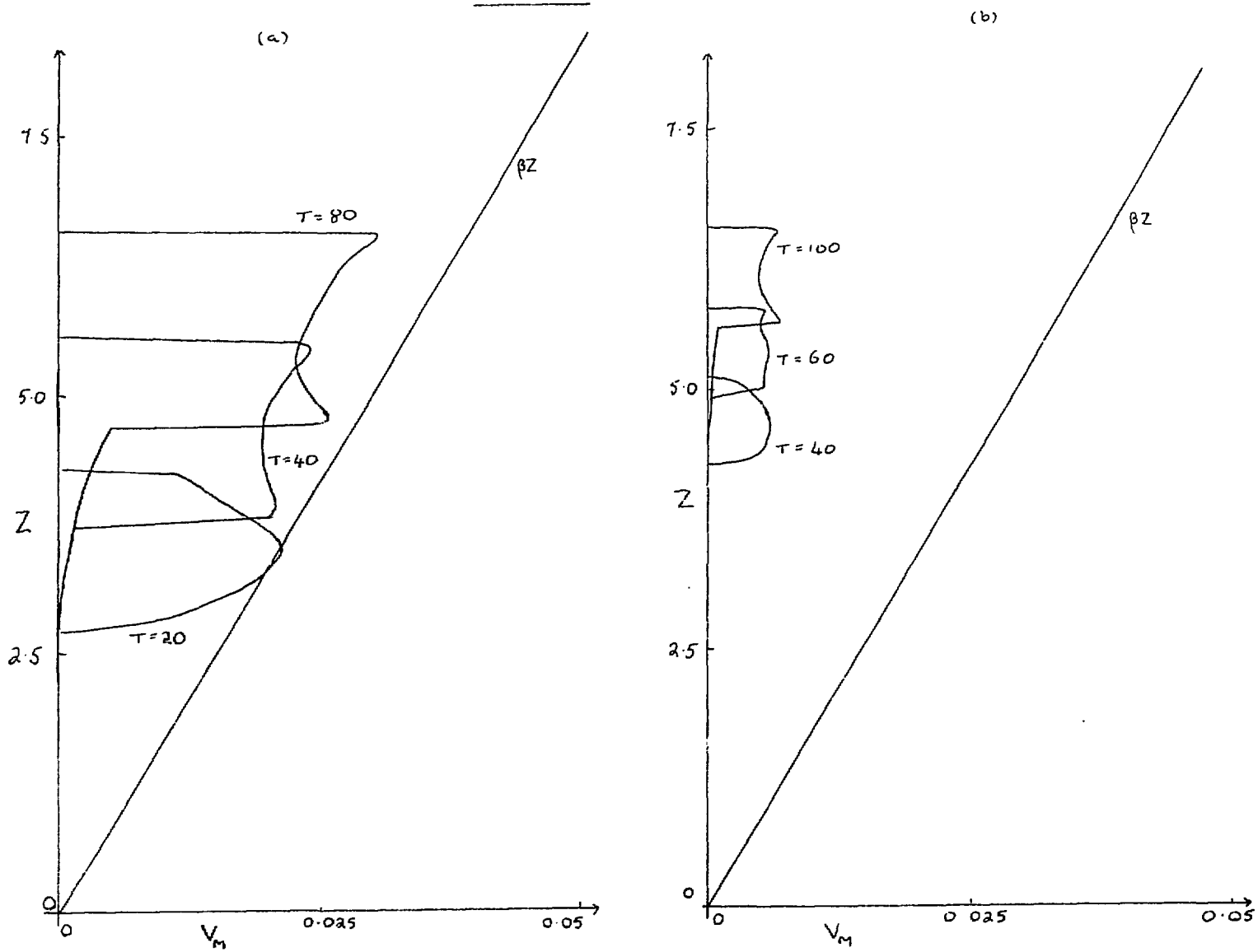
(a)
7·5
5·0
2·5
0
Z
βZ
T = 80
T = 40
T = 20
0
0·025
0·05
V_M
(b)
7·5
5·0
2·5
0
Z
βZ
T = 100
T = 60
T = 40
0
0 025
0·05
V_M

Figure 8

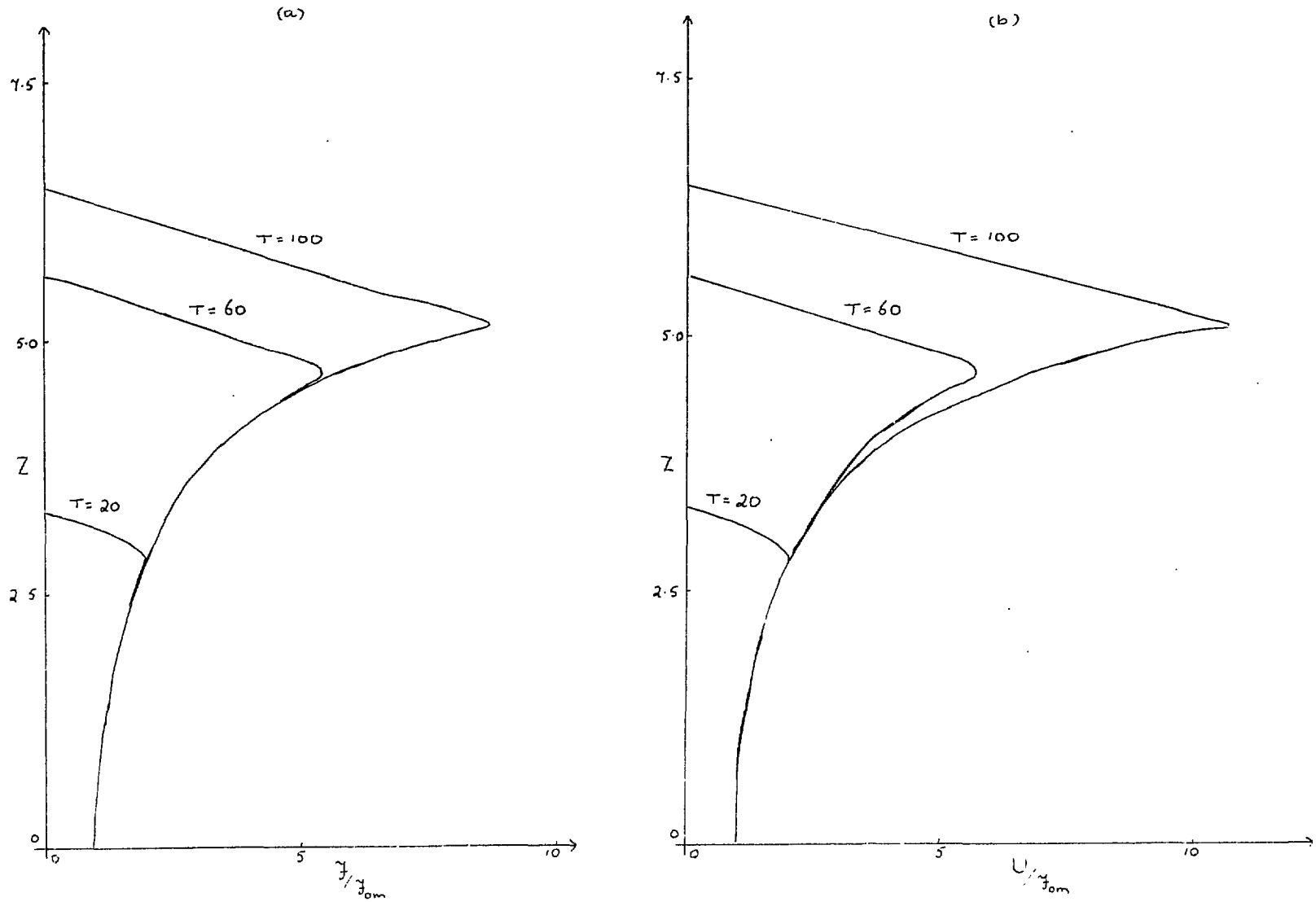
(a)
7·5
5·0
2·5
0
Z
T = 100
T = 60
T = 20
0
5
10
γ/γ_{om}
(b)
7·5
5·0
2·5
0
Z
T = 100
T = 60
T = 20
0
5
10
U/γ_{om}

Figure 9

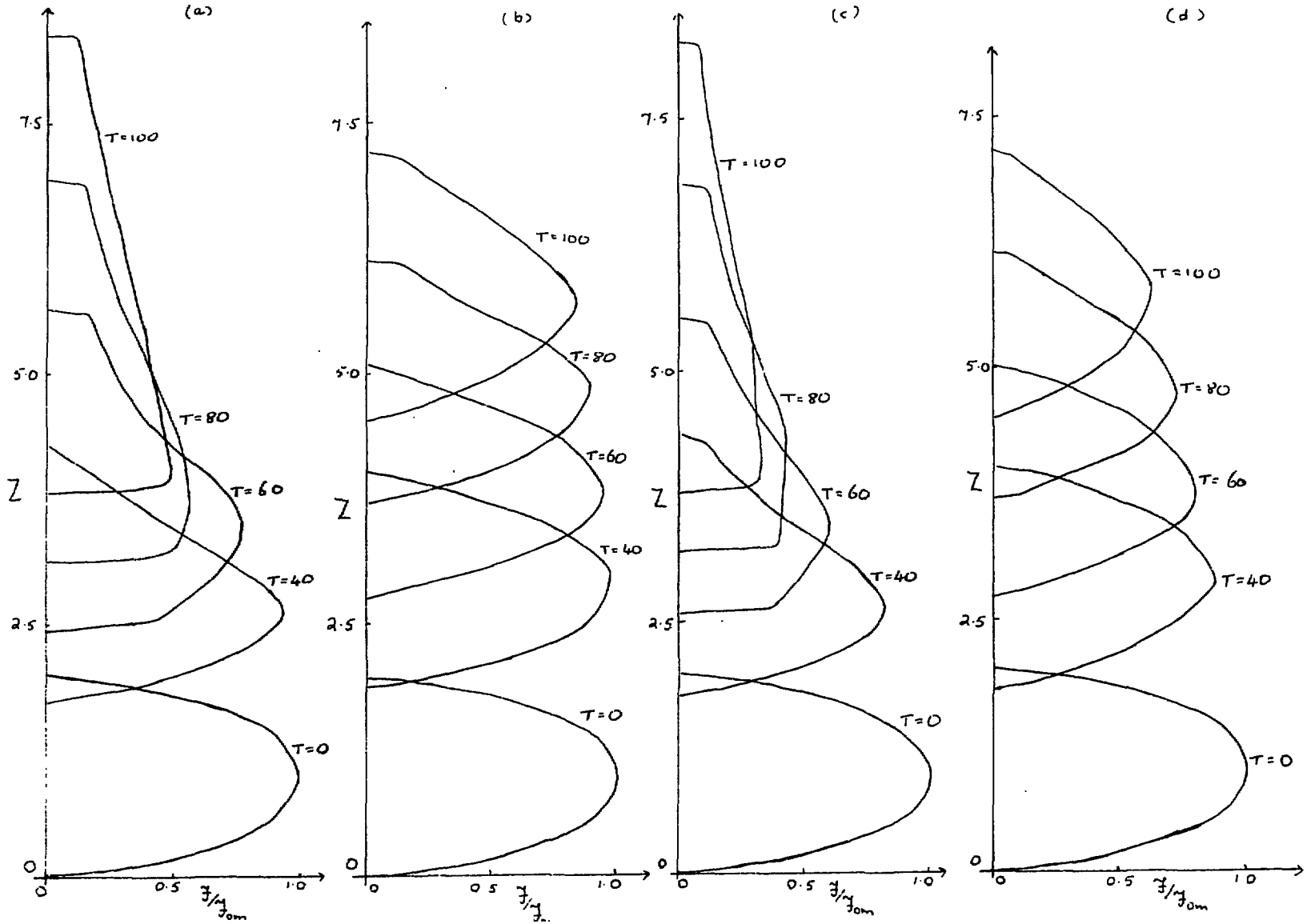

Figure 10

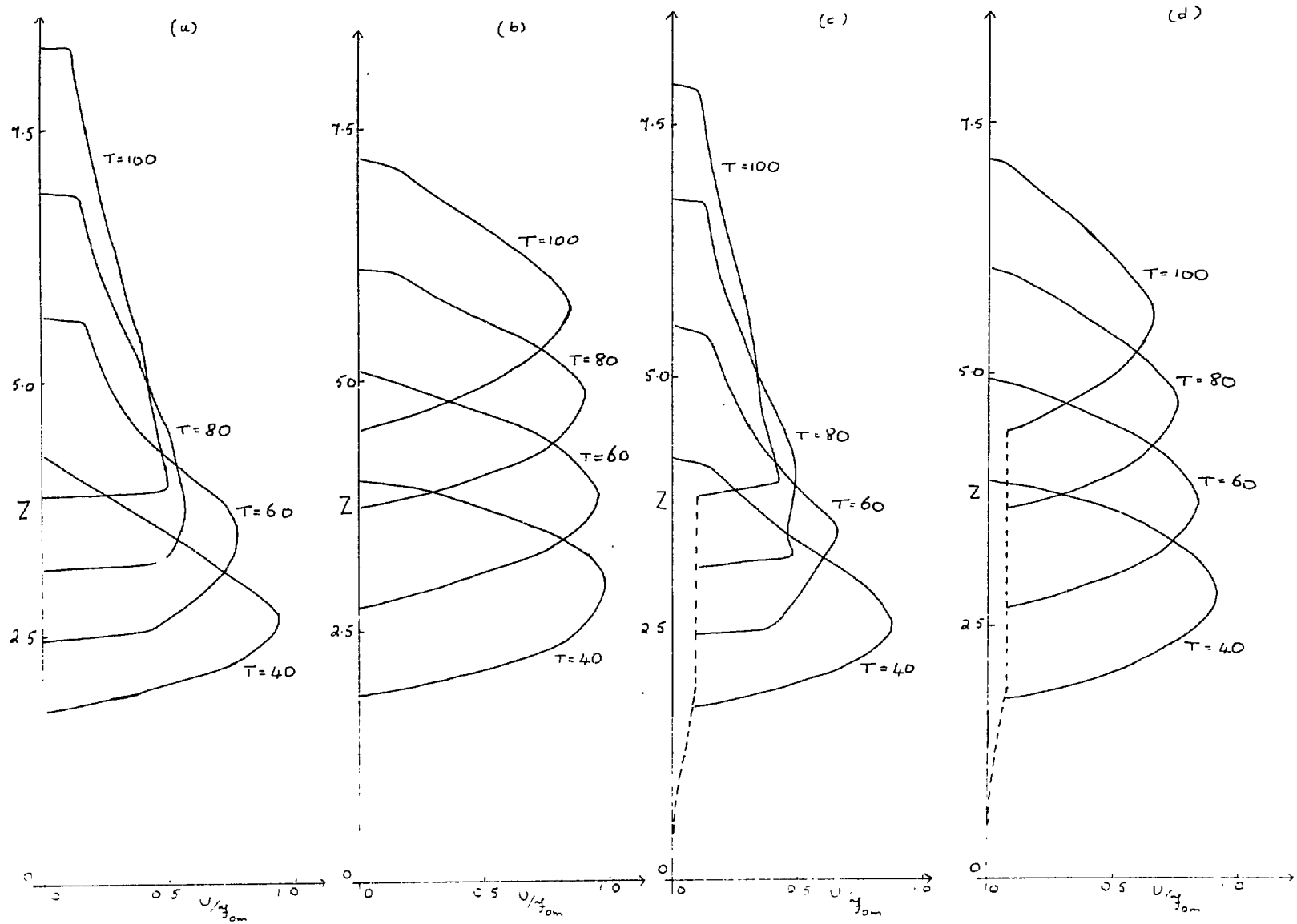

Figure 11

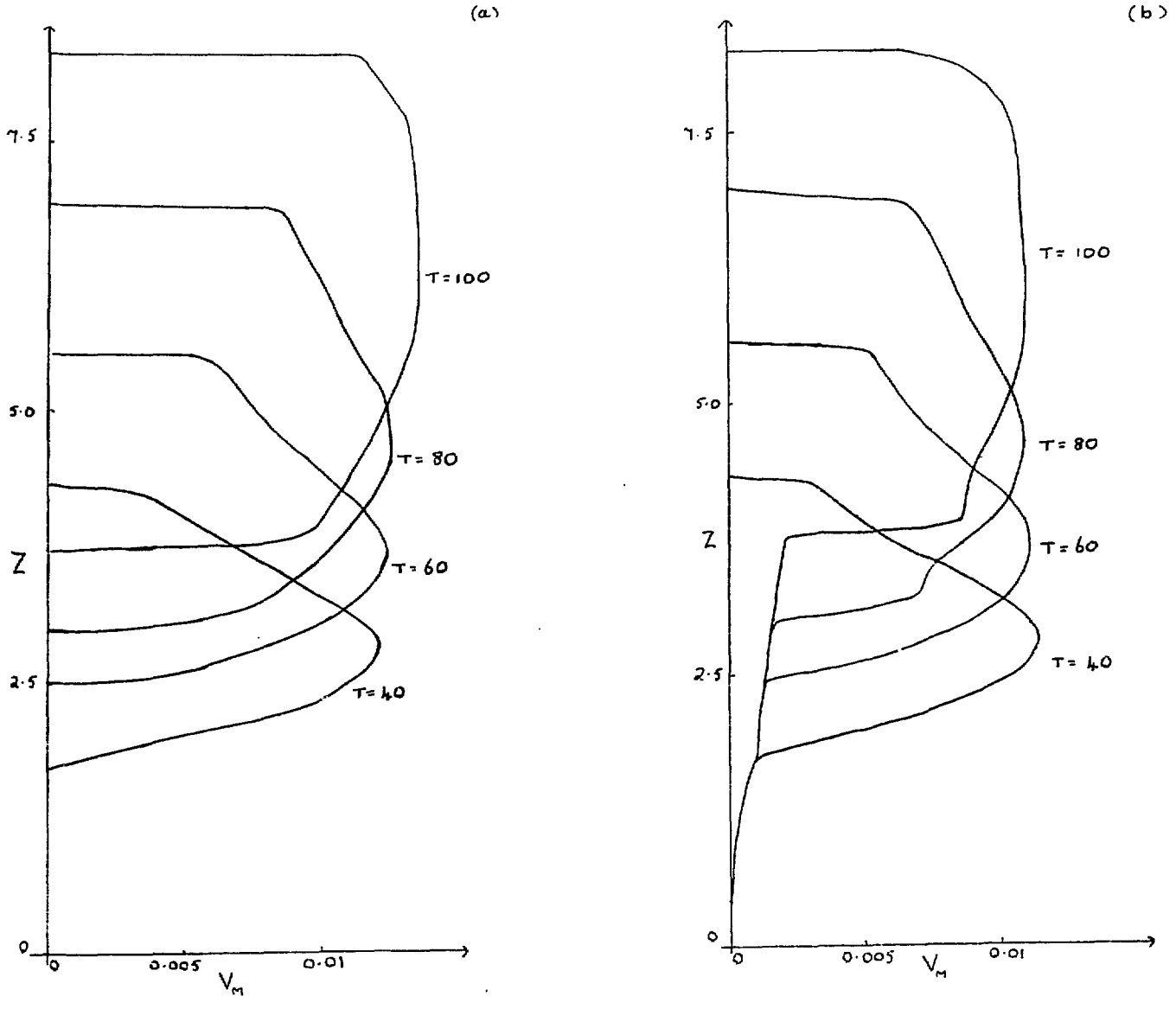
(a)
7·5
5·0
2·5
0
Z
T=100
T=80
T=60
T=40
0
0·005
0·01
V_M
(b)
7·5
5·0
2·5
0
Z
T=100
T=80
T=60
T=40
0
0·005
0·01
V_M

Figure 12

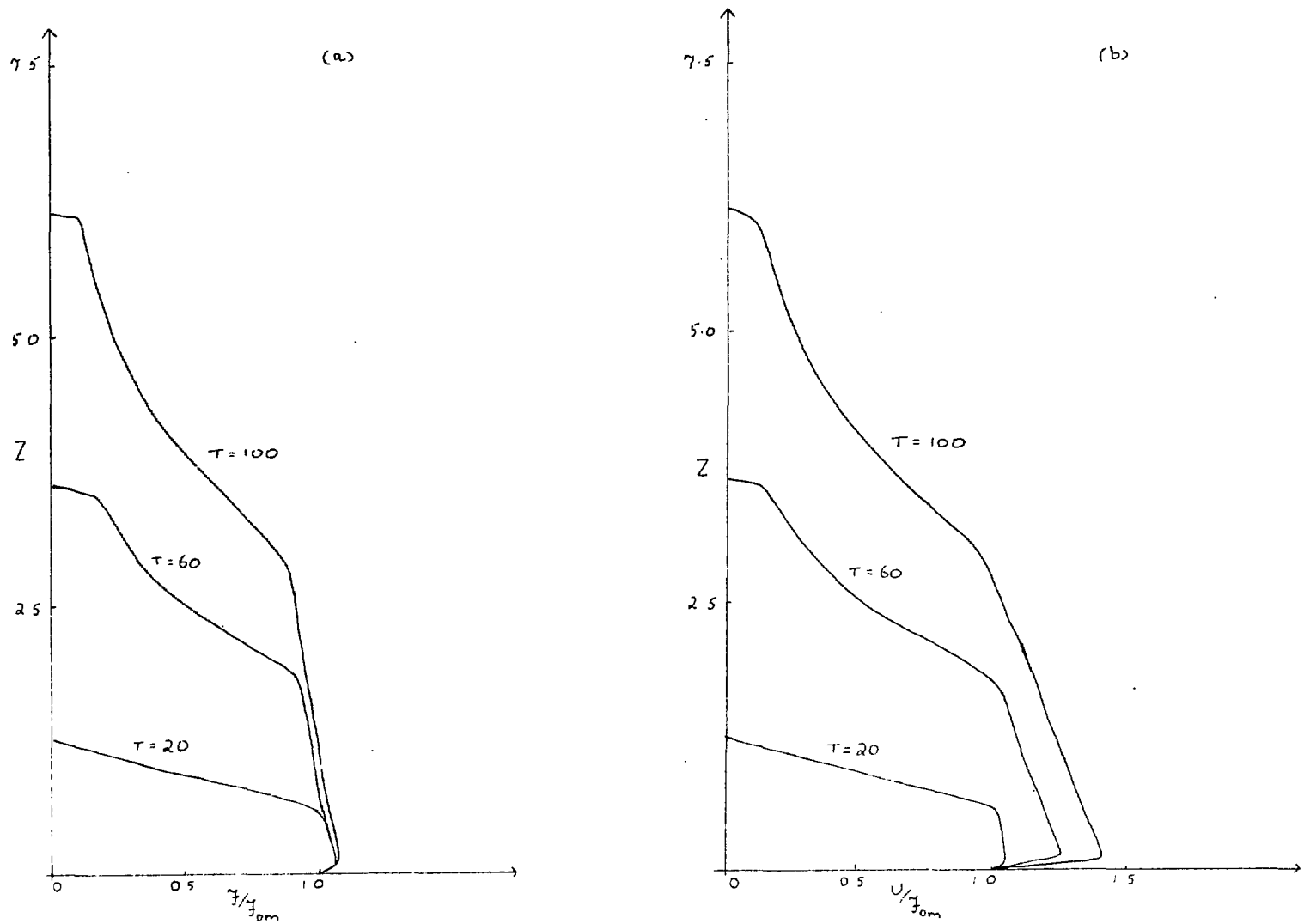
(a)
7.5
5.0
2.5
Z
T = 100
T = 60
T = 20
0
0.5
1.0
J/J_{om}
(b)
7.5
5.0
2.5
Z
T = 100
T = 60
T = 20
0
0.5
1.0
1.5
U/J_{om}